Supporting Information

Inter-atomic Electronic Interactions Enables by Rh Single Atoms/$CuCo_2S_4$@MoS_2 Core-Shell Heterostructure for High-efficiency Solar-assisted Water Splitting

Xinfeng Zhu[a], Kaixuan Dong[a], Dinh Chuong Nguyen[a], Sampath Prabhakaran[a], Do Hwan Kim[b], Duy Thanh Tran[a], Nam Hoon Kim[a*], Joong Hee Lee[a,c*]

[a] Department of Nano Convergence Engineering, Jeonbuk National University, Jeonju, Jeonbuk, 54896, Republic of Korea.

[b] Division of Science Education, Department of Energy Storage/Conversion Engineering, Jeonbuk National University, Jeonju-si, Jeonbuk 54896, Republic of Korea

[c] Carbon Composite Research Center, Department of Polymer-Nano Science and Technology, Jeonbuk National University, Jeonju, Jeonbuk, 54896, Republic of Korea.

*Corresponding author: nhk@jbnu.ac.kr and jhl@jbnu.ac.kr.

Experimental

Synthesis of Rh SAs/MoS_2 sample. The 3D NF was treated with ethanol, 3M HCl, and DI water for 20 min each via ultrasonic prior to placing in the 50 mL Teflon-lined stainless-steel autoclave. A reactant solution of 0.1 g of $Na_2MoO_4.2H_2O$, 0.15 g of NH_2CSNH_2, and 0.01 g of $N_6Na_3O_{12}Rh$ was also poured into the Teflon container containing the cleaned 3D NF. The hydrothermal reaction was performed at 200 °C for 8 h. After the temperature was dropped to room temperature, the Rh SAs/MoS_2 sample was taken out, repeatedly washed with DI water and ethanol, and finally dried at 60 °C.

Synthesis of Pt/C and RuO_2 electrodes. 5 mg of Pt/C or RuO_2 powders was dissolved in 500 μL of isopropyl alcohol and 0.5 μL of Nafion solution under sonicating for 1 h to prepare electrode ink. Then, the obtained ink was dropped on the cleaned nickel foam to form Pt/C or RuO_2 working electrode for comparison.

Density Functional Theory (DFT). DFT calculations were performed using the Vienna Ab initio Simulation Package (VASP) [S1] to identify the active sites of the optimal catalyst on its surface. Grimme's DFT-D3 functional and the Perdew-Burke-Ernzerhof (PBE) exchange-correlation functional [S2] were employed within a semi-empirical GGA type theory framework. Ion-electron interactions were explored using the projector augmented wave method (PAW) implemented in VASP [S3], with a plane-wave basis set cut-off energy of 400 eV. Convergence criteria were set at 10^{-5} eV for energy and 0.02 eV $Å^{-1}$ for Hellman–Feynman forces. The crystalline structures were positioned in the center, with equal vacuum exposure on both the top and bottom. The "VASPKIT" script within the VASP program was utilized to generate a KPOINT file for calculating the k-point mesh [S4]. The influence of Gibbs free energy (ΔG_{*H}) on the catalytic performance in the HER process, as indicated by previous studies [S5], was examined.

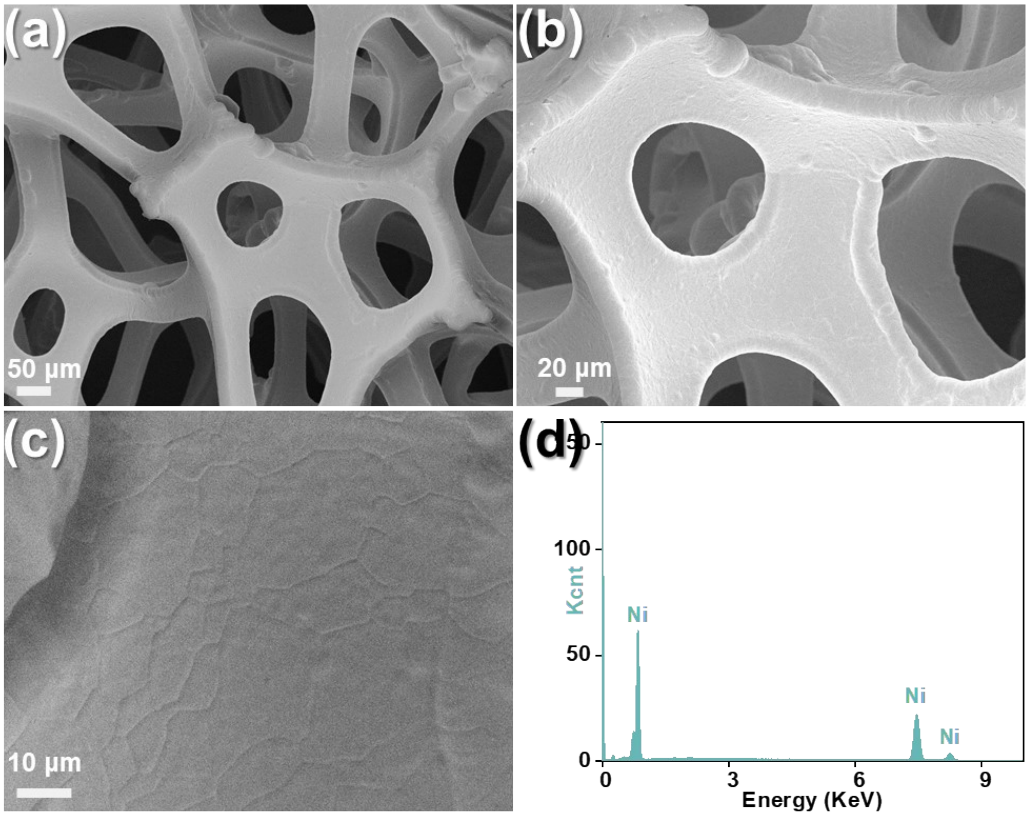

Fig. S1. (a)-(c) SEM images at different magnifications and (d) EDS spectrum of 3D NF.

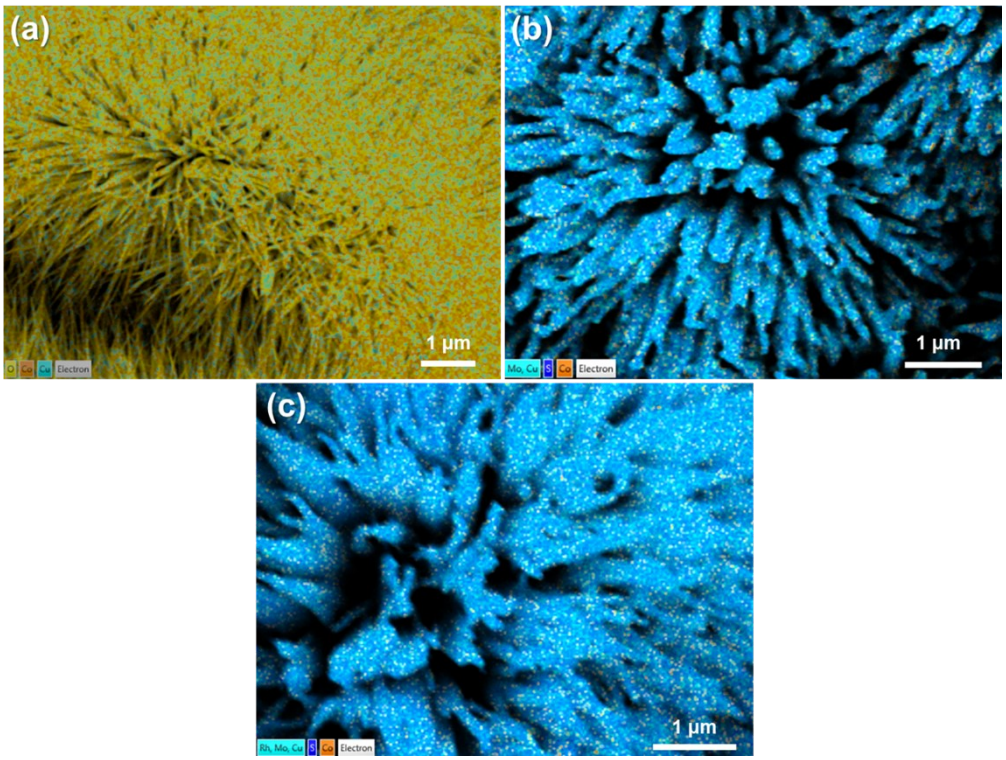

Fig. S2. EDS patterns of (a) CuCo-OH; (b) $CuCo_2S_4$@MoS_2; and (c) Rh SAs/$CuCo_2S_4$@MoS_2.

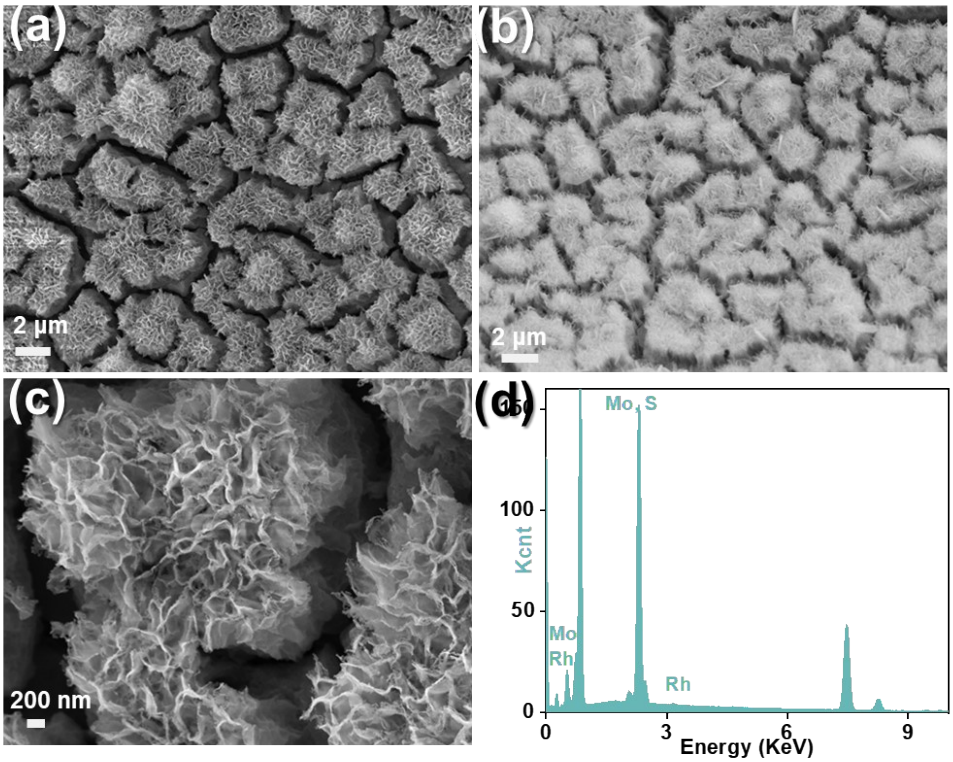

Fig. S3. (a)-(c) SEM images with different magnifications and (d) EDS spectrum of Rh SAs/MoS_2.

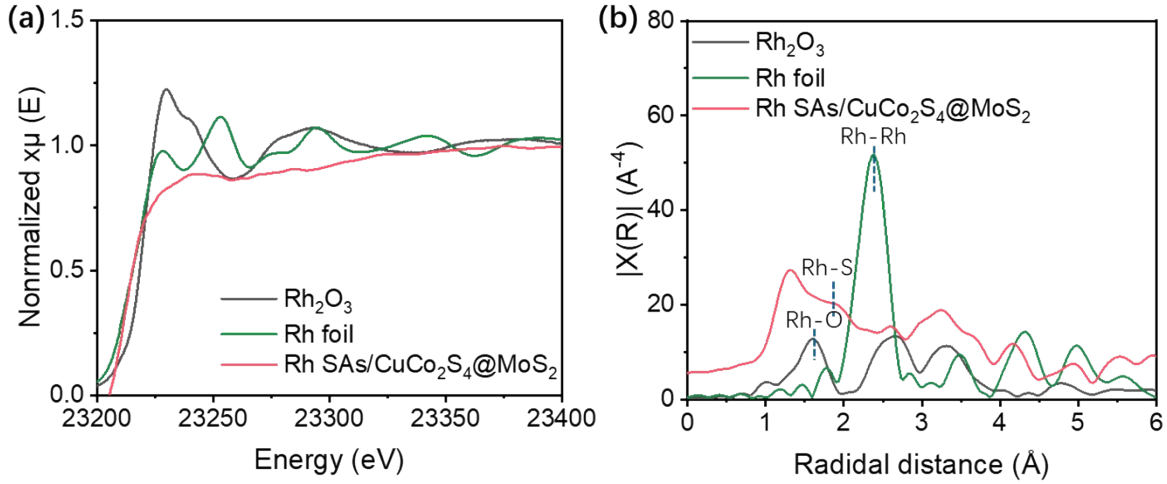

Fig. S4. XAS analysis of the Rh SAs/$CuCo_2S_4$@MoS_2 material as compared to that of Rh metal and Rh_2O_3 referred from open access sources from MDR [S6,S7].

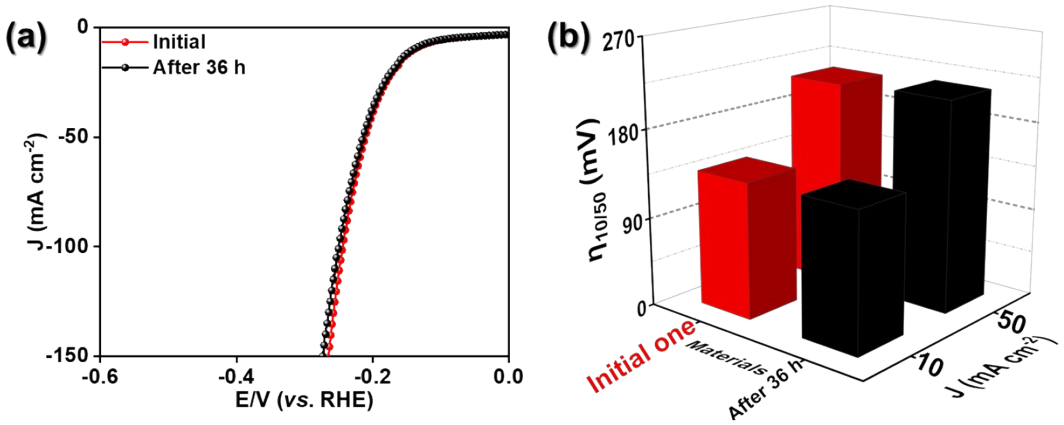

Fig. S5. (a) LSV curves and (b) comparison of overpotential at 10 and 50 mA cm^{-2} of Rh SAs/$CuCo_2S_4$@MoS_2 recorded before and after stability testing for the HER.

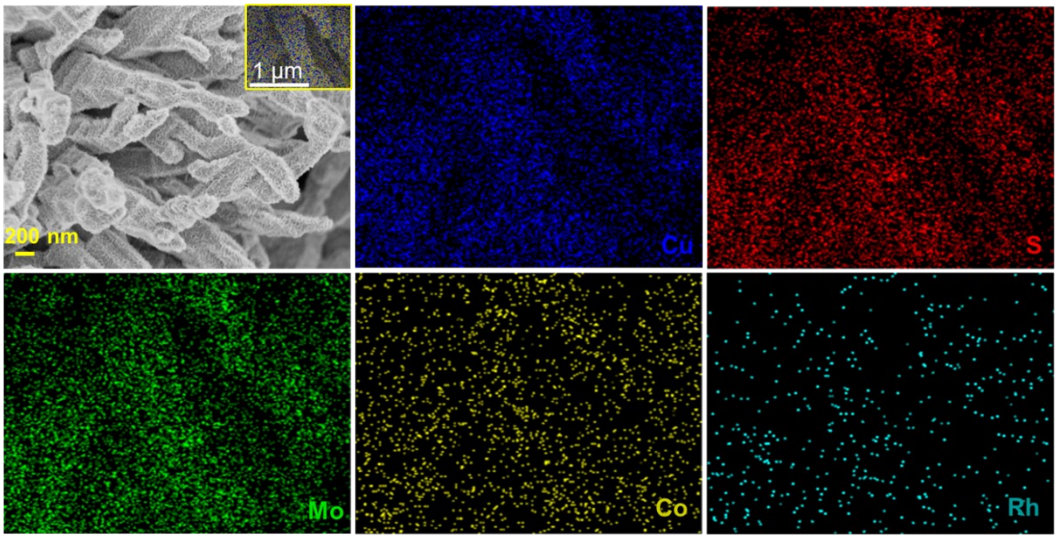

Fig. S6. (a) SEM and (b)-(f) EDS mapping images of the post-HER Rh SAs/$CuCo_2S_4$@MoS_2.

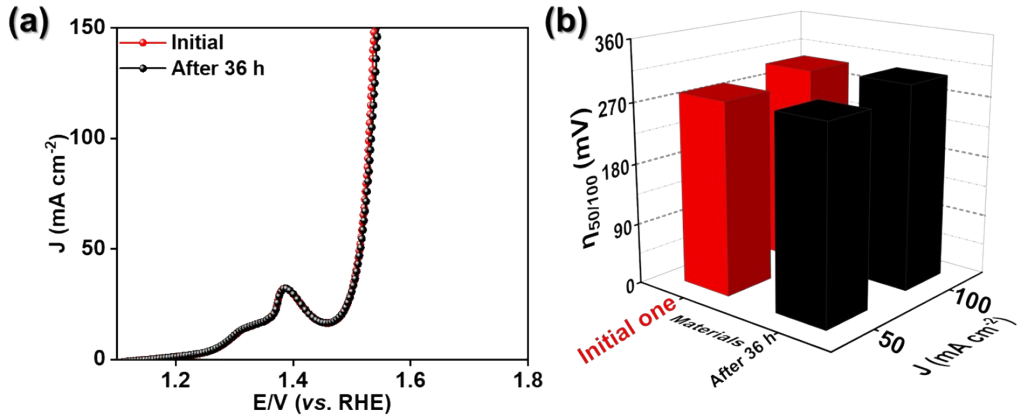

Fig. S7. (a) LSV curves and (b) comparison of overpotential at 10 and 50 mA cm^{-2} of Rh SAs/$CuCo_2S_4$@MoS_2 recorded before and after stability testing for the OER.

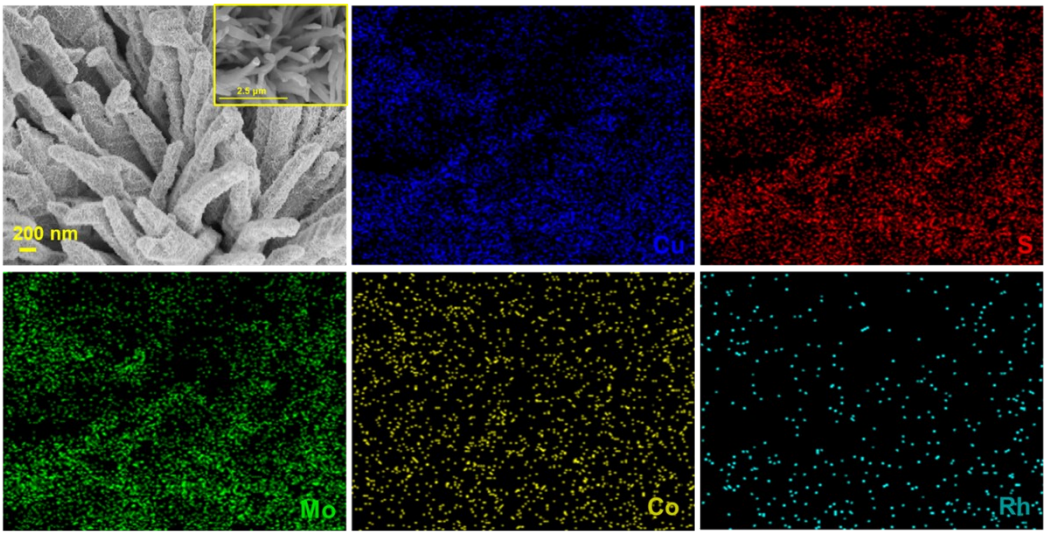

Fig. S8. (a) SEM and (b)-(f) EDS mapping images of the post-OER Rh SAs/$CuCo_2S_4$@MoS_2.

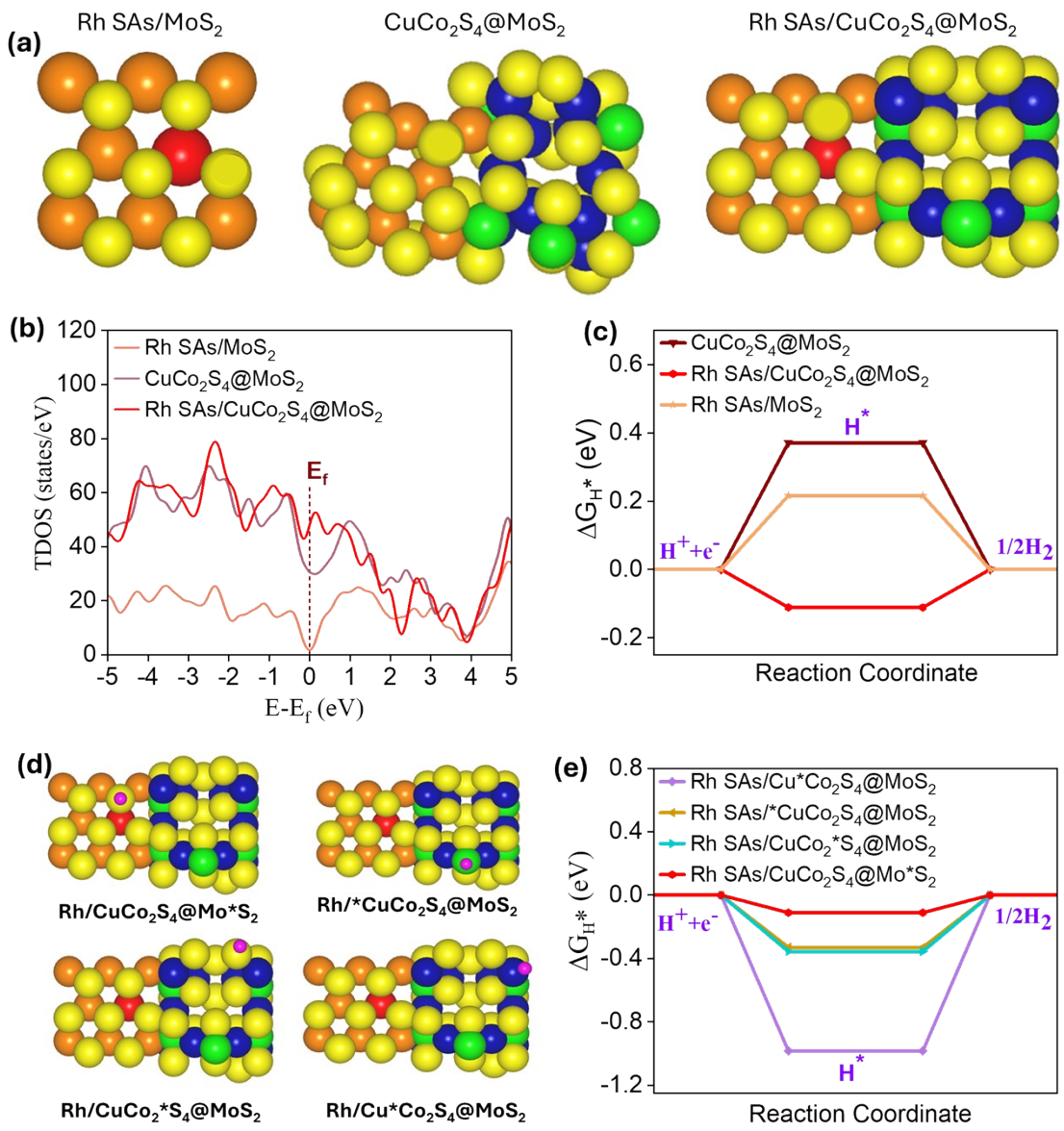

Fig. S9. (a) Structure models of different materials; (b) TDOS and (c) Free adsorption energy of different materials; (d) Adsorption of hydrogen on possible sites of Rh SAs/$CuCo_2S_4$@MoS_2 structure for HER and (e) corresponding free adsorption energy of different active sites for HER.

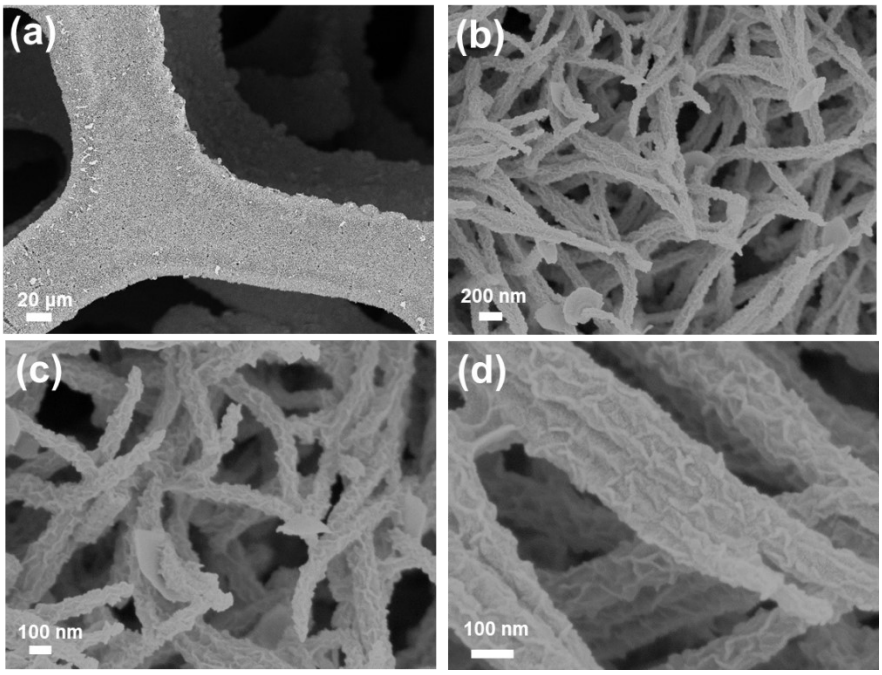

Fig. S10. (a-d) SEM images at different magnifications of the post-OER Rh SAs/$CuCo_2S_4$@MoS_2 after 36 h stability test for overall water splitting.

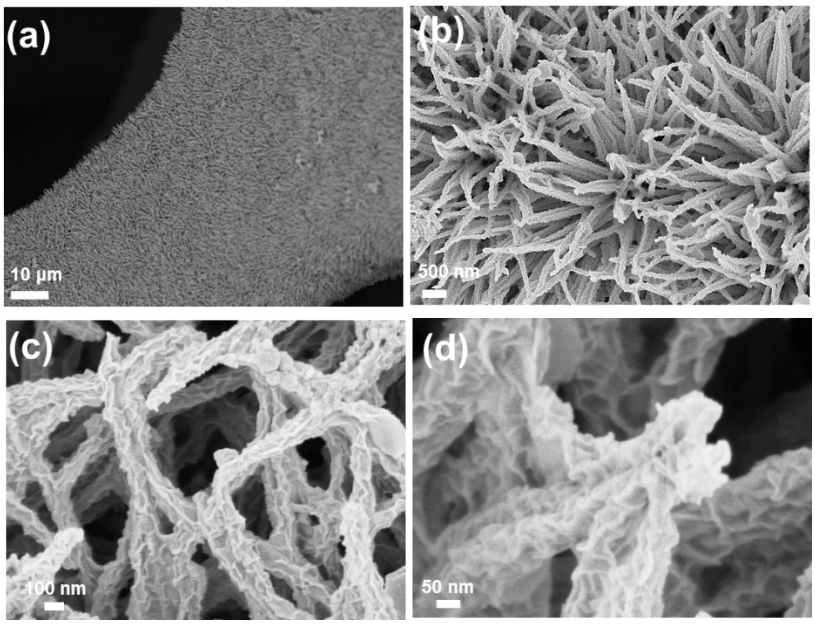

Fig. S11. (a-d) SEM images at different magnifications of the post-HER Rh SAs/$CuCo_2S_4$@MoS_2 after 36 h stability test for overall water splitting.

.

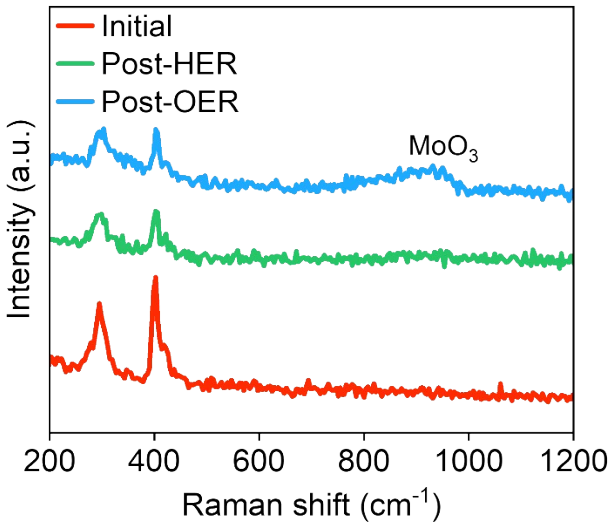

Fig. S12. Raman spectra of Rh SAs/$CuCo_2S_4$@MoS_2 before and after HER and OER stability testing.

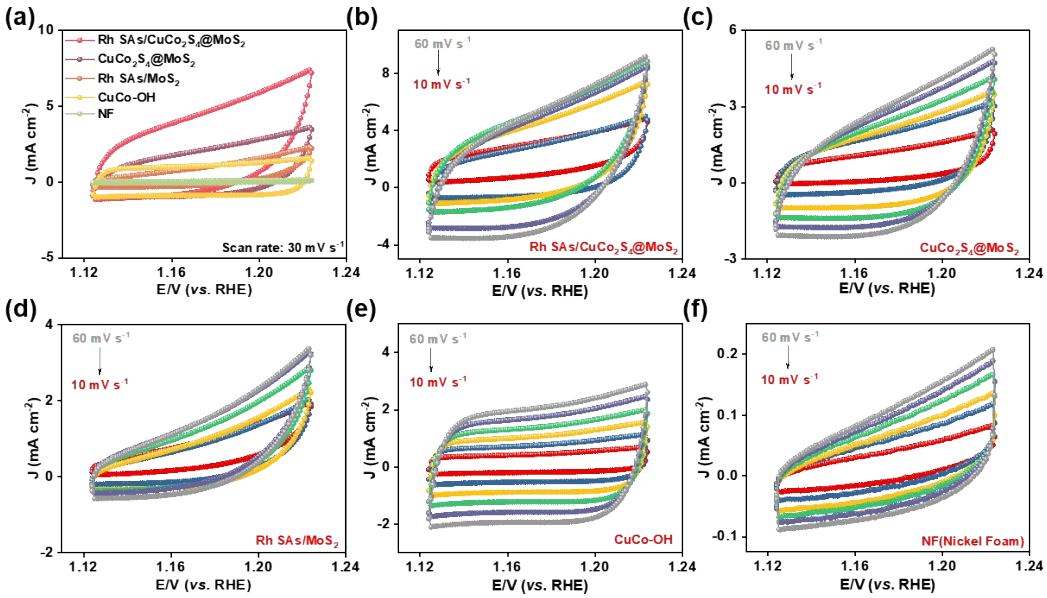

Fig. S13. (a) CV curves at scan rate of 30 mV s^{-1} of Rh SAs/$CuCo_2S_4$@MoS_2, $CuCo_2S_4$@MoS_2, Rh SAs/MoS_2, CuCo-OH, and 3D NF. (b)-(f) CV curves at different scan rates of Rh SAs/$CuCo_2S_4$@MoS_2, $CuCo_2S_4$@MoS_2, Rh SAs/MoS_2, CuCo-OH, and 3D NF, respectively.

Table S1. Comparison of recently reported electrocatalysts for the HER.

Catalysts	Overpotential at 10 mA cm^{-2} (mV)	References
Co/CoO@NC@CC	152	Chem. Eng. J., 2021, 414, 128804
Te/FeNiOOH-NC	167	Acs. Appl. Mater. Inter., 2021, 13, 10972-10978
POM@ZnCoS/NF	170	Adv. Funct. Mater., 2021, 31, 2106147
CoP@FeCoP/NC	141	Chem. Eng. J., 2021, 403, 126312
Mo_2NiB_2	160	Small, 2022, 18, 2104303
NiS_2/MoS_2/CNTs	149	Appl. Surf. Sci., 2023, 615, 156309
Ni_3S_2/MoS_2	166	Int. J. Hydrogen Energy, 2022, 47, 8165– 8176
Ru-doped CuO/MoS_2	198	ACS Appl. Nano Mater., 2021, 4, 8, 7675–7685
CoNiN@NiFe LDH	150	Appl. Surf. Sci., 2021, 570, 151182
CoFeCr LDH	201	Nanomaterials, 2022, 12, 1227
CoFeCr/NF	159	J. Colloid Interf. Sci., 2021, 604, 767-775
CoP@FeCoP/NC YSMPs	141	Chem. Eng. J., 2021, 403, 126312
NiFeP/CC	129	Chem. Eng. J., 2021, 420, 129972
NiMo@$Ni(OH)_2MoO_x$	160	Renew. Energy, 2022, 191, 370-379
Co_9S_8@CoMoS-P	240	Int. J. Hydrogen Energy, 2024, 49,

		805-815
rGO@SN-$CoNi_2S_4$	142.6	Rare Met., 2022, 41, 911–920
Co_3O_4/MoS_2	260	Int. J. Hydrogen Energy, 2024, 49, 805-815
Co_2FeO_4@rGO	320	Int. J. Hydrogen Energy, 2022, 47, 33919-33937
Cu_2O/RGO	142	ACS Appl. Nano Mater., 2022, 5, 11, 17271–17280
β-MnO_2-VO_2(B)/2D-rGO	178	J. Phys. Chem. C, 2022, 126 (7), 3419– 3431
Rh SAs/$CuCo_2S_4$@MoS_2	**140.27**	**This work**

Table S2. Comparison of recently reported electrocatalysts for the OER.

Catalysts	Overpotential at 100 mA cm^{-2} (mV)	References
$Ni(CN)_2/NiSe_2$	470	Adv. Mater., 2022, 34, 2104405
$Co_2P/CoP@Co@NCNT$	360	Chem. Eng. J., 2022, 430
$CoTe_2/CoP$	354	Appl. Catal. B- Environmental., 2023, 329, 122551
MoS_2/Cu	320	Mater. Design., 2021, 204
MoS_2/NiFe LDH	330	Chinese Chem. Lett., 2022, 33, 4761-4765
γ-FeOOH	362	Adv. Mater., 2021, 33,2005587.
$CoS_2/MoS_2@CC$	340	Chem. Sus. Chem. 2021, 14, 699-708
$MoS_2/NiS_2/CC$-2	384	Electro. Chimica., Acta. 2021, 385
$(Fe, Ni)S_2@MoS_2/NiS_2$	380	Int. J. Hydrogen Energy, 2022, 47, 11143-11152
MoS_2-Mo_2C	309	Nano Energy, 2021, 88, 106277
NiFe-LDH/MoS_2-Ni_3S_2/NF	347	Inorg. Chem., 2023, 62, 16, 6428–

		6438
MoS_2-AB	420	Nano Energy, 2022, 92, 106707
NiS_2/MoS_2/CNTs	500	Appl. Surf. Sci., 2023, 615, 156309
Ni_3S_2/MoS_2	411	Int. J. Hydrogen Energy, 2022, 47, 8165– 8176
$MoS_2@Co_3S_4$/NC	464	J. Colloid nterface Sci., 2023,649, 125-131
CoS_2/MoS_2@PPy/NF	324	ACS Sustainable Chem. Eng., 2024, 12, 1, 235–247
Ru-doped CuO/MoS_2	433	ACS Appl. Nano Mater., 2021, 4, 8, 7675–7685
Rh/CoAl LDHs	390	ACS Appl. Nano Mater., 2023, 6, 9, 7984–7991
P,Cu-$Co_{0.85}Se$/NF	300	J. Alloys Compd., 2021, 889, 31, 161696
Te-$CoMoO_3$@C	299	Inorg. Chem. Front., 2022, 9, 3788-3796
Rh SAs/$CuCo_2S_4$@MoS_2	**297**	**This work**

Table S3. Comparison of recently reported electrocatalysts for the overall water splitting.

Catalysts	Overpotential at 10 mA cm^{-2} (mV)	References
$Ru_{0.7}Co_{0.3(+,-)}$	1.59	J. Power Sources, 2021, 514, 230600
Ce-doped CoMoP/MoP@$C_{(+,-)}$	1.59	Energy Fuels, 2021, 35, 14169
Cr-CoP/$CP_{(+,-)}$	1.59	Chem. Eng. J., 2021, 425, 130651
Ni-Mo_2C/$NC_{(+,-)}$	1.59	Appl. Catal. B, 2021, 292, 120168
NiCoP/CoFeP@ $NF_{(+,-)}$	1.61	Int. J. Hydrogen Energy, 2021, 46, 37872
CoFeP@NSOC-$400_{(+,-)}$	1.62	Ceram Int., 2021,47, 12843
Al, Fe-CoP/$RGO_{(+,-)}$	1.66	Chem. Eng., 2021, 421, 127856
Co_9S_8/Cu_2S/$CF_{(+,-)}$	1.6	ACS Appl. Mater. Interfaces, 2021, 13, 8, 9865
Ni_3S_2/$MoS_{2(+,-)}$	1.62	Int. J. Hydrogen Energy, 2022, 47, 8165– 8176
NiS_2/MoS_2/$CNTs_{(+,-)}$	1.73	Appl. Surf. Sci., 2023, 615, 156309
Ru-doped CuO/$MoS_{2(+,-)}$	1.68	ACS Appl. Nano Mater., 2021, 4, 8, 7675–7685
$NiFe_2O_4$@N-$rGO_{(+,-)}$	1.67	Energy & Fuels, 2022, 36, 9, 4911-4923
IrO_2@MnO_2/$rGO_{(+,-)}$	1.60	ACS Sustainable Chemistry & Engineering, 2022, 10, 46,

		pp.15068-15081
$(NiCo)S_2/NCNF_{(+,-)}$	1.61	Inorganic Chemistry, 2022, 61, 36, pp.14436-14446
$Co_3S_4/MoS_2\ NR_{(+,-)}$	1.62	Inorganic Chemistry Frontiers, 2022, 9, 10, 2139-2149
$MnxCoyO_4/Ti_{(+,-)}$	1.60	Dalton Transactions, 2022, 51, 23, 9085-9093
CeO_2-$Co(OH)_{2(+,-)}$	1.62	Int. J. Hydrogen Energy, 2022, 47, 16, 9593-9605
$CuO@Cu_3P_{(+,-)}$	1.75	Int. J. Hydrogen Energy, 2022, 47, 16, 9593-9605
$CoO{-}Co_9S_{8(+,-)}$	1.66	Chem. Electro. Chem., 2022, 9, 3, e202101566
$CoS_2/MoS_{2(+,-)}$	1.66	Chemistry Select, 2022, 7, 47, e202202700
Rh SAs/$CuCo_2S_4$@MoS_2 (+/-)	**1.589**	**This work**

Table S4. Comparison of the STH conversion efficiency between $CuCo_2S_4$@Rh-MoS_2 $NSs_{(+,-)}$ with other previous reports.

Catalysts	STH (%)	References
$Co_2P/Mo_2C@NC_{(+,-)}$	18.1	Appl. Catal. B, 2022, 310, 121354.
NiMoP//NiFeP	14.0	Appl. Catal. B, 2021, 297, 120434.
S-$NiFeOOH_{(+,-)}$	7.2	J. Energy Chem., 2022, 64, 364.
Co_9S_8 @MoS_2||Pt/C	13.6	Appl. Catal B-Environmental., 2022, 309
NiFeNb-0.25/NF	15.56	Electrochim. Acta., 2022, 429, 140947.
CoNiLDH/$CoFe_2O_4$//$CoFe_2O_4$	12.7	J. Power Sources, 2022, 538, 231536.
Co_9S_8@MoS_2//Pt/C	13.6	Appl. Catal. B, 2022, 309, 121272.
FeNiWOx||Pt/C	13.9	Appl. Energy Mater., 2022, 5, 8241-8253
H-FeNiP	5.6	J. Mater. Chem. A., 2021, 9, 1221-1229
S-$NiFeOOH_{(+,-)}$	7.2	Energy Chem., 2022, 64, 364-371
$Ni@C_{(+,-)}$	8.1	J. Mater. Chem. A., 2021, 9, 223828-23840
S-$(Co,Fe)OOH_{(+,-)}$	13.0	Nanoscale Adv., 2021, 3, 6386-6394.

NiFeMo-NF||NiFeMo-NP	13.8	ACS Sustain. Chem. Eng., 2021, 9, 14070-14078
NiMoFe/Cu $NW_{(+,-)}$	11.0	Chem. Commun., 2022, 58, 1569-1572
NiMoP/NF-NiFeP/NF $OWS_{(+,-)}$	14.0	Appl. Catal. B-Environmental., 2021, 297, 120434
CoNi@MoS_2-PdSARuSA$_{(+,-)}$	17.7	ACS Sustainable Chem. Eng., 2023, 11, 17, 6688–6697
NiMoP/$NiFeP_{(+,-)}$	14.3	Appl. Catal. B, 2021, 297, 120434
$MoNi_4/MoO_{x(+,-)}$	11.28	J. Mater. Chem. A, 2023, 11, 10346-10359
Rh SAs/$CuCo_2S_4$@MoS_2 (+/-)	**19.12**	**This work**

References

[S1] G. Kresse and J. Furthmüller, *Phys. Rev. B*, 1996, **54**, 11169.

[S2] S. Ehrlich, J. Moellmann, W. Reckien, T. Bredow, S. Grimme, *Chemphyschem*, 2011, **12**, 3414-3420.

[S3] Peter E. Blöchl, O. Jepsen, and O. K. Andersen, *Phys. Rev. B*, 1994, **49**, 16223.

[S4] V. Wang, N. Xu, J.-C. Liu, G. Tang, W.-T. Geng, *Comp. Phys. Commun*., 2021, **267**, 108033.

[S5] L. Yan, B. Zhang, J. Zhu, Y. Li, P. Tsiakaras, P. K. Shen, *Appl. Catal. B: Environ*., 2020, **265**, 118555.

[S6] https://mdr.nims.go.jp/concern/datasets/ww72bf03x?locale=en

[S7] https://mdr.nims.go.jp/concern/datasets/wh246w12w?locale=en